

Quantum spin models of commensurate p -wave magnets

GiBaik Sim^{1,*} and Stephan Rachel^{1,†}

¹*School of Physics, The University of Melbourne, Parkville, VIC 3010, Australia*

(Dated: March 2, 2026)

The p -wave magnet has emerged as a new type of magnetism exhibiting odd-parity, time-reversal-symmetric spin splitting in momentum space, and has attracted considerable interest as a promising platform for spintronic applications. However, the theoretical understanding of the fundamental mechanism responsible for stabilizing this phase remains limited. In this work, we identify a microscopic interacting model that realizes the p -wave magnet as its ground state. We first introduce a Hubbard model and derive the corresponding low-energy spin Hamiltonian. At the classical level, we find that the p -wave magnet is stabilized but remains energetically degenerate with competing noncoplanar states. Quantum fluctuations lift this degeneracy, selecting the p -wave magnet as the unique ground state. The resulting electronic structure exhibits finite spin accumulation via the Edelstein effect, highlighting the potential of p -wave magnetism for spintronic applications. We further discuss the relevance of our theory to quasi-two-dimensional honeycomb magnets such as $\text{Ni}_2\text{Mo}_3\text{O}_8$. Our findings establish the possibility of spontaneous p -wave magnetism.

Introduction. — The spin texture of electronic bands in momentum space is closely intertwined with the symmetry of magnetic order in real space.[1–4] In standard ferromagnets, broken time-reversal symmetry lifts spin degeneracy and generates uniform spin splitting across the Brillouin zone, giving rise to an even-parity s -wave spin polarization on the Fermi surface. [5] Momentum-dependent spin splitting can also emerge in magnets with more complex order. In particular, altermagnets (d -wave magnets) [6–13] exhibit sign-changing spin polarization in momentum space, reflecting the underlying crystalline symmetry of their collinear magnetic structure. [14–17]

Earlier attempts to realize odd-parity, time-reversal-symmetric p -wave spin splitting focused on an angular momentum $l=1$ spin Pomeranchuk instability of a Fermi liquid. [18–21] However, this mechanism was later shown to be prohibited by the spin conservation law. [22, 23] More recent studies circumvent this constraint by generating p -wave spin splitting from noncollinear magnetic states. [24–26] Within this framework, the p -wave magnet has been interpreted as a commensurate spiral order whose commensurability restores time-reversal symmetry when combined with lattice translations.

In parallel, significant progress has been achieved on both experimental and theoretical fronts. Experimentally, p -wave magnetic order has been directly confirmed in both insulating and metallic systems: NiI_2 [27] exhibits an electrically switchable multiferroic p -wave state, while $\text{Gd}_3(\text{Ru}_{0.95}\text{Rh}_{0.05})_4\text{Al}_{12}$ [28] hosts a commensurate coplanar spin helix characteristic of a metallic p -wave magnet. On the theoretical side, first-principles calculations [24, 25, 29] and symmetry-based classifications [30–33], have predicted various forms of odd-parity magnetism in correlated materials. These include the p -wave candidate CeNiAsO [24, 25, 34, 35] and several Fe-based compounds [29, 36–38] hosting higher-order odd-parity spin textures. Moreover, Floquet-engineered schemes have been proposed to dynamically induce such

odd-parity spin splitting. [39–41]

Despite these advances, microscopic realizations within interacting Hubbard-type or spin models remain largely unexplored [42, 43]. Establishing such models is crucial for understanding the fundamental stabilization mechanisms of p -wave magnetic order and for being able to access excitation spectra. In this work, we identify Hubbard models that realize the p -wave magnet as their ground state in the strong-coupling limit. Starting from a Hubbard model, we derive the low-energy spin Hamiltonian and find that the p -wave magnet is stabilized but remains energetically degenerate with competing noncoplanar states at the classical level. To determine the ground state in the quantum regime, we investigate the corresponding spin-1/2 model using matrix product state simulations based on infinite density-matrix renormalization group (iDMRG). We demonstrate that quantum fluctuations lift the classical degeneracy and select the p -wave magnet as the unique quantum ground state. Furthermore, we show that the resulting minimal tight-binding model exhibits finite spin accumulation manifested in the Edelstein effect, revealing the potential relevance of p -wave magnetism for spintronics applications.

Hubbard model on honeycomb lattice. — We first introduce a variant of the Hubbard model on the two-dimensional honeycomb lattice, which is written as

$$H = t \sum_{\langle ij \rangle \in \gamma} c_i^\dagger [\cos \theta + i \sin \theta \hat{\mathbf{d}}_\gamma \cdot \boldsymbol{\sigma}] c_j + U \sum_i n_{i,\uparrow} n_{i,\downarrow}, \quad (1)$$

where $c_i^\dagger \equiv (c_{i,\uparrow}^\dagger, c_{i,\downarrow}^\dagger)$ is the two-component spinor, and the Pauli matrices $\boldsymbol{\sigma}$ act on the spin degree of freedom. The first term describes nearest-neighbor hopping, where θ quantifies the ratio between spin-independent and spin-dependent hopping amplitudes, and $\hat{\mathbf{d}}_\gamma$ specifies the form of spin-dependent hopping on the $\gamma = x, y, z$ bonds (see inset of Fig. 1(a) for the bond labeling). The second term represents the usual onsite Coulomb repulsion. We

consider two representative configurations of $\hat{\mathbf{d}}_\gamma$:

$$(i) \quad \hat{\mathbf{d}}_\gamma = \hat{\gamma}, \quad (2)$$

$$(ii) \quad \hat{\mathbf{d}}_x = (1, 0, 0), \hat{\mathbf{d}}_y = C_{3z}\hat{\mathbf{d}}_x, \hat{\mathbf{d}}_z = C_{3z}^2\hat{\mathbf{d}}_x \quad (3)$$

where C_{3z} denotes a threefold rotation by 120° about the z axis. In the strong-coupling limit $U/t \rightarrow \infty$, Eq. (1) can be projected onto the subspace with one electron per site, leading to an effective spin Hamiltonian,

$$H_s = J \sum_{\langle ij \rangle \in \gamma} [\cos 2\theta \mathbf{S}_i \cdot \mathbf{S}_j + \sin 2\theta \hat{\mathbf{d}}_\gamma \cdot (\mathbf{S}_i \times \mathbf{S}_j)] \\ + (1 - \cos 2\theta)(\hat{\mathbf{d}}_\gamma \cdot \mathbf{S}_i)(\hat{\mathbf{d}}_\gamma \cdot \mathbf{S}_j), \quad (4)$$

where $J = 4t^2/U$. [44, 45] The first term denotes the isotropic Heisenberg exchange, while the second and third terms represent the Dzyaloshinskii–Moriya (DM) and Kitaev-type anisotropic interactions, respectively. Hereafter, we restrict our analysis to configuration (i) [Eq. (2)]; results for configuration (ii) [Eq. (3)] are provided in the End Matter. For $\theta = 0$, the model reduces to the antiferromagnetic Heisenberg limit, whose ground state is the well-known Neel order. In contrast, $\theta = \pi/2$ corresponds to the Heisenberg-Kitaev limit (with $J_K/J_H = -2$), extensively studied in the context of Kitaev materials, where the system stabilizes a collinear zigzag state.[46–52] Accordingly, models described by Eq. (1) are often termed Kitaev–Hubbard models in the literature. Related Kitaev-Hubbard models have been studied in condensed-matter and cold-atom contexts. [53–57] The key distinction to these works is that the spin-dependent hopping term in Eq. (1) is imaginary. Thus, the non-interacting part of the Hamiltonian preserves time-reversal symmetry, and generates the DM interactions in the strong-coupling limit.

Classical spin model.— To gain initial insight into the nature of the magnetic ground state, we first analyze the classical spin model, before proceeding to the quantum case. In the classical limit, quadratic spin Hamiltonians can be treated exactly within the Luttinger–Tisza (LT) framework, where the classical ground state is obtained by minimizing the Fourier-transformed interaction matrix. [58–60] When the lowest-energy LT eigenmodes satisfy the local hard-spin constraint $|\mathbf{S}_i| = 1$ —either individually or through a linear combination of degenerate eigenmodes—the LT solution yields the exact classical ground state. In the entire parameter regime explored in this work, the LT solution satisfies the hard-spin constraint. Iterative minimization [59] is employed in a complementary manner to resolve how the degenerate LT eigenmodes combine into a physical state that satisfies the hard-spin constraint. The resulting classical phase diagram of the model in Eq. (4) is shown in Fig. 1(a) (see Sec. I of the Supplemental Material). For $0 < \theta < 0.85$, the system favors an incommensurate spiral state, which can be identified from the eigenvalue spectrum of the LT

interaction matrix. Fig. 1(c) displays the LT spectrum for $\theta = \pi/5$, where the minimum of the lowest band lies between the high-symmetry points Γ and M . The corresponding eigenmode at this wave vector satisfies the hard-spin constraint, indicating that the system stabilizes an incommensurate spiral state in this parameter regime.

For $0.85 \leq \theta < \pi/2$, the minimum of the lowest LT band is located exactly at the M point, as shown in Fig. 1(d) for $\theta = \pi/3$, and the corresponding eigenmode satisfies the hard-spin constraint. In this regime, the system stabilizes a noncollinear zigzag state, which corresponds exactly to a *p-wave magnet*. The relative canting angle ϕ between the spin-polarization axes S_A^z and S_B^z of the two crystallographic sublattices, plotted in Fig. 1(b), quantifies this noncollinearity: $\phi = 0$ corresponds to a collinear zigzag state, while a finite ϕ signals the emergence of the *p-wave magnet*. The canting angle decreases continuously as θ approaches $\pi/2$, as shown in Fig. 1(a). In this phase, the magnetic unit cell is doubled relative to the crystallographic unit cell, as depicted in Fig. 1(b). The *p-wave* state is, however, energetically degenerate with noncoplanar states constructed as a superposition of three symmetry-related degenerate eigenmodes whose ordering wave vectors lie at the M points connected by the C_{3z} rotation (see Sec. I of the Supplemental Material for details). In Figs. 1(e,f), we present the nearest-neighbor spin correlators $\langle S_i^z S_j^z \rangle$ and $\langle S_i^z S_j^x \rangle$ for the *p-wave magnet*. Like S_i^z , the spin component $S_{i \in A, B}^x$ along the local \hat{x} axis is defined separately on sublattices A and B . The correlation pattern indicates that spins are collinear within their respective local frames but rotate relative to each other in the global frame, giving rise to a globally noncollinear yet strictly coplanar configuration. In contrast, the competing multi- Q noncoplanar states display finite out-of-plane correlations, $\langle S_i^z S_j^x \rangle$, and exhibit a qualitatively distinct correlation pattern (see Sec. I of the Supplemental Material for details).

It is expected that quantum order-by-disorder effects favor the single- Q coplanar state over the multi- Q noncoplanar states. [61, 62] Below, we move on to the quantum model and investigate whether a *p-wave magnet* is indeed selected by quantum fluctuations.

Quantum spin model.— To clarify which features of the classical phase diagram survive in the quantum regime, we perform iDMRG [63, 64] calculations on the spin-1/2 model. The simulations employ a unit cell containing 48 sites and bond dimensions up to 2000, providing a reliable description of the phases found at the classical level, except for the incommensurate spiral states (see Sec. II of the Supplemental Material for details). The results are presented in Fig. 2(a). A first-order phase transition is indicated by a kink in the ground-state energy per site ϵ , where the first derivative $\partial\epsilon/\partial\theta$ changes sign at $\theta \simeq 0.85$. To characterize the state stabilized in $0.85 \leq \theta < \pi/2$, we compute the nearest-neighbor spin

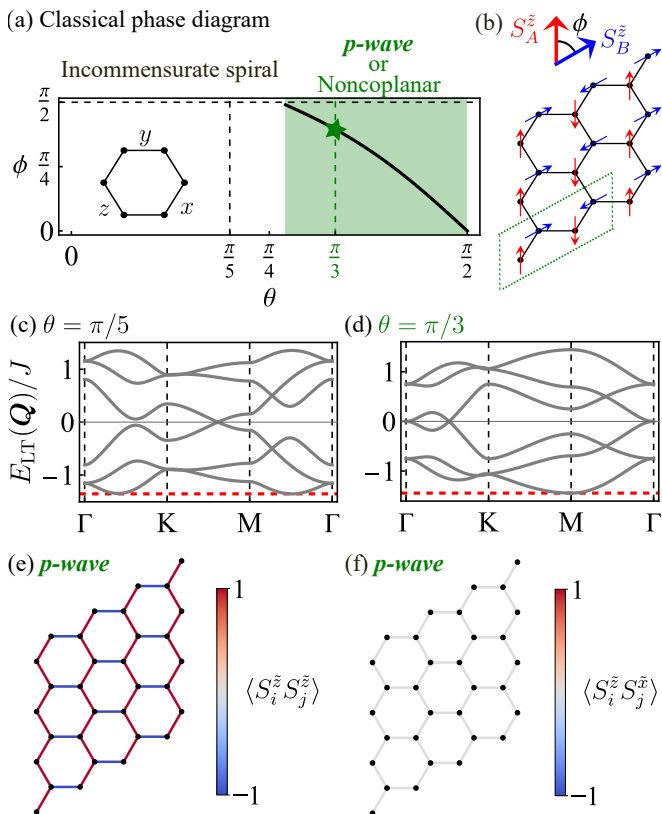


FIG. 1. (a) Classical phase diagram of the model given in Eq. (4) for $\hat{\mathbf{d}}_\gamma = \hat{\gamma}$. For $0.85 \leq \theta < \pi/2$, the model stabilizes the p -wave magnetic and noncoplanar states, which are energetically degenerate. (b) Spin configuration of the p -wave magnet, which is noncollinear. The canting angle ϕ between the local spin-polarization axes S_A^z and S_B^z quantifies the noncollinearity between the two sublattices. The magnetic unit cell, indicated by the dashed green outline, is twice as large as the crystallographic unit cell. (c,d) Eigenvalue spectra of the LT interaction matrix for $\theta = \pi/5$ and $\pi/3$. The minimum of the lowest-energy band is located at an incommensurate wave vector for the former and at the M point for the latter. (e,f) Nearest-neighbor spin correlators $\langle S_i^z S_j^z \rangle$ and $\langle S_i^z S_j^x \rangle$ for the p -wave magnet.

correlators $\langle S_i^z S_j^z \rangle$ and $\langle S_i^z S_j^x \rangle$, as shown in Figs. 2(b,c). The correlation patterns exhibit the same structure as in the classical case shown in Figs. 1(e,f): spins remain collinear within their respective local reference frames but form a globally noncollinear yet coplanar configuration. The resulting magnetic structure has a four-site magnetic unit cell, as shown in Fig. 2(b), consistent with the p -wave magnet. Thus, quantum fluctuations lift the classical degeneracy and select the p -wave magnet as the ground state.

Band structure and Edelstein effect.— The p -wave magnet possesses distinctive symmetry properties. It breaks spatial inversion P as well as the combined PT symmetry, where \mathcal{T} denotes time reversal. At the same time, it preserves the composite symmetry $\mathcal{T}T(\mathbf{t}_1)$, where

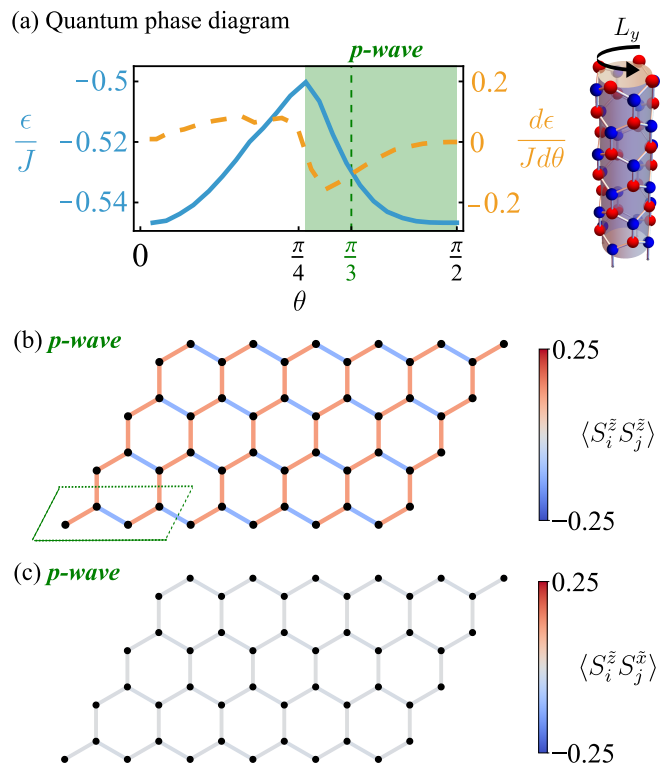


FIG. 2. (a) Quantum phase diagram of the spin-1/2 model in Eq. (4) for $\hat{\mathbf{d}}_\gamma = \hat{\gamma}$. The simulations are performed on an infinite cylinder with $L_x \times L_y \times 2 = 6 \times 4 \times 2$ sites per unit cell, where L_x is repeated along the infinite direction and L_y is the periodic circumference. Quantum fluctuations select the p -wave magnet over the noncoplanar states that are energetically degenerate at the classical level. (b,c) Nearest-neighbor spin correlators $\langle S_i^z S_j^z \rangle$ and $\langle S_i^z S_j^x \rangle$ for the p -wave magnet at $\theta = \pi/3$. The magnetic unit cell is indicated by the dashed green outline in (b).

\mathbf{t}_1 is one of the lattice translation vectors and $T(\mathbf{t}_1)$ is the corresponding translation operator. This symmetry preserves time-reversal symmetry in momentum space, enforcing the relation $E(\mathbf{k}, \mathbf{S}) = E(-\mathbf{k}, -\mathbf{S})$. In addition, the system retains a spin symmetry $[C_2^\perp || \mathbf{t}_1]$, where C_2^\perp denotes a 180° spin rotation about the axis perpendicular to the spin plane. The corresponding symmetry $[C_2^\perp || E]$ in momentum space enforces that only the spin component along the C_2^\perp rotation axis remains finite, resulting in a spin polarization strictly aligned with this axis. Together, these two symmetries constrain the spin polarization in momentum space to satisfy

$$E(\mathbf{k}, S^\perp) = E(-\mathbf{k}, -S^\perp). \quad (5)$$

We introduce a minimal tight-binding model to illustrate the electronic properties of the p -wave magnet on the honeycomb lattice. The model is given by

$$H_p = t \sum_{\langle ij \rangle} c_i^\dagger c_j + J_d \sum_i c_i^\dagger [\hat{\mathbf{m}}_i^p \cdot \boldsymbol{\sigma}] c_i, \quad (6)$$

where \hat{m}_i^p denotes the site-dependent local spin polarization of the p -wave magnet shown in Fig. 1(b), and J_d quantifies the coupling between the itinerant electrons and the localized moments. The electronic band structure of Eq. (6) is shown in Fig. 3(a), plotted within the first Brillouin zone of the crystallographic unit cell (the number of bands is doubled due to zone folding). The resulting band dispersion clearly exhibits p -wave-type spin splitting, satisfying the relation given in Eq. (5). Moreover, we find that the spin-degenerate Dirac cones present at $J_d = 0$ [Fig. 3(b)] split into pairs of spin-polarized Dirac cones once $J_d > 0$, as shown in Fig. 3(c). These Dirac cones remain stable until J_d reaches a critical value J_d^c , where Dirac cones with opposite spin polarization annihilate in pairs. On the other hand, the Dirac cones are immediately gapped once sublattice symmetry is broken—for instance, by introducing a sublattice-dependent onsite potential.

The odd-parity spin-momentum locking enables an electric current to induce a net spin polarization—a magnetoelectric response known as the Edelstein effect [65–68]. To evaluate this effect, we employ the Kubo formalism within the constant relaxation time approximation. We focus on the component of the response that is linear in the applied electric field, written as $\delta S_\alpha = \chi_{\alpha\beta} E_\beta$, where δS_α is the induced spin polarization, E_β is the electric field, and $\chi_{\alpha\beta}$ is the response tensor. Time-reversal even and odd components of $\chi_{\alpha\beta}$ are derived in Ref. [65, 66]:

$$\chi_{\alpha\beta}^{\text{even}} = \frac{-e\hbar}{\pi} \sum_{m,n,\mathbf{k}} \frac{\text{Re} \left[\langle \psi_{\mathbf{k},m} | \hat{S}_\alpha | \psi_{\mathbf{k},n} \rangle \langle \psi_{\mathbf{k},n} | \hat{v}_\beta | \psi_{\mathbf{k},m} \rangle \right] \Gamma^2}{[(E_F - E_{\mathbf{k},m})^2 + \Gamma^2][(E_F - E_{\mathbf{k},n})^2 + \Gamma^2]}, \quad (7)$$

$$\chi_{\alpha\beta}^{\text{odd}} = 2e\hbar \sum_{\substack{m:\text{occ.} \\ n:\text{unocc.}, \mathbf{k}}} \text{Im} \left[\langle \psi_{\mathbf{k},n} | \hat{S}_\alpha | \psi_{\mathbf{k},m} \rangle \langle \psi_{\mathbf{k},m} | \hat{v}_\beta | \psi_{\mathbf{k},n} \rangle \right] \times \frac{\Gamma^2 - (E_{\mathbf{k},m} - E_{\mathbf{k},n})^2}{[(E_{\mathbf{k},m} - E_{\mathbf{k},n})^2 + \Gamma^2]^2}. \quad (8)$$

Here, $|\psi_{\mathbf{k},n}\rangle$ denotes the Bloch eigenstate of band n with wave vector \mathbf{k} , whose energy is $E_{\mathbf{k},n}$, and E_F is the Fermi level. The quantity $e > 0$ is the elementary charge, \hat{S}_α is the spin operator, and $\hat{v}_\beta = \frac{1}{\hbar} \partial H_p(\mathbf{k}) / \partial k_\beta$ is the group-velocity operator. The parameter Γ characterizes disorder broadening and is related to the relaxation time by $\tau = \hbar / (2\Gamma)$. As χ^{odd} represents a Fermi-surface property that is odd under time-reversal symmetry, it is allowed only in systems that explicitly break the time-reversal symmetry, which include ferromagnets and certain non-collinear antiferromagnets [68–71]. In our case of the p -wave state, this quantity vanishes, as also confirmed by our numerical calculations, in agreement with the result in Ref. [25].

For the model in Eq. (6), $\chi_{\perp x}^{\text{even}}$ is the only nonvanishing component of the Edelstein response tensor. This corresponds to a current-induced spin accumulation oriented

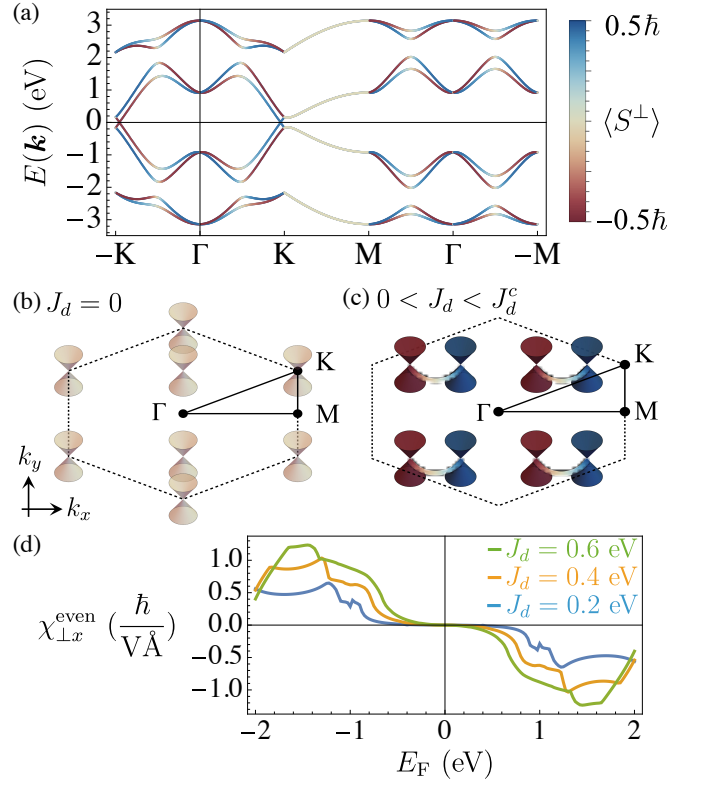


FIG. 3. (color online) (a) Band spectrum of the model in Eq. (6) with parameters $t = 1$ eV and $J_d = 0.6$ eV. The bands exhibit p -wave type spin polarization in momentum space, consistent with Eq. (5). Spin degeneracy is restored along the high-symmetry Γ - M line at the Brillouin-zone boundary. (b) At $J_d = 0$, four spin-degenerate Dirac cones appear at the Fermi level within the first Brillouin zone of the crystallographic unit cell. (c) For $0 < J_d < J_d^c$, eight spin-polarized Dirac cones appear at the Fermi level in the first Brillouin zone of the crystallographic unit cell. At the critical coupling $J_d = J_d^c$, Dirac cones annihilate in pairs and a gap opens. Pairs of Dirac cones are connected by guiding lines for visualization. (d) Calculated $\chi_{\perp x}^{\text{even}}$ for $t = 1$ eV and $\Gamma = 0.01$ eV with $J_d = 0.2, 0.4$, and 0.6 eV. The magnitude of $\chi_{\perp x}^{\text{even}}$ increases with J_d .

along the band spin-polarization axis when an electric field is applied along the x direction. In Fig. 3(d), we plot $\chi_{\perp x}^{\text{even}}$ as a function of the Fermi level E_F for $t = 1$ eV, $\Gamma = 0.01$ eV, and several values of J_d . As J_d increases, Dirac cones with opposite spin polarization are displaced further in opposite k_x directions, resulting in an enhanced response magnitude. The particle-hole symmetry observed in the response is consistent with the band structure shown in Fig. 3(a). To indicate the typical scale of the response, we note that comparable susceptibility values have been reported in other magnetic systems. For example, a p -wave magnet on a square lattice studied in Ref. [25] yields $\chi^{\text{even}} \simeq 2\hbar/\text{V}\text{\AA}$ for $\Gamma = 0.01$ eV. Within our minimal model description, the Edelstein response lies within a similar range.

Summary and outlook.— In summary, we have identified Hubbard models that realizes a p -wave magnet with a commensurate ordering wave vector as its ground state. In the strong-coupling limit $U/t \rightarrow \infty$, the corresponding low-energy spin Hamiltonian stabilizes a p -wave magnetic state that is energetically degenerate with a competing noncoplanar state at the classical level. In the quantum limit $S = 1/2$, this degeneracy is lifted by quantum fluctuations, which select the p -wave magnet. We then introduce a minimal model in which itinerant electrons couple to this commensurate noncollinear magnetic texture and analyze the resulting band structure. The model exhibits a defining feature of p -wave magnetism: an odd-parity spin-polarized band dispersion across the Brillouin zone. Furthermore, we compute the Edelstein response and find a finite symmetry-allowed component of the response tensor $\chi_{\perp x}^{\text{even}}$, demonstrating current-induced spin accumulation along the band spin-polarization axis.

Although our main analysis focuses on case (i) defined by Eq. (2), case (ii) specified in Eq. (3) is directly relevant to the honeycomb magnet $\text{Ni}_2\text{Mo}_3\text{O}_8$, which hosts effective spin-1 moments on Ni^{2+} ions. In this compound, neighboring Ni ions occupy inequivalent tetrahedral and octahedral oxygen environments, breaking inversion symmetry on each nearest-neighbor bond.[72, 73] This local asymmetry permits finite DM interactions with DM vectors that correspond to the pattern in Eq. (3).[74] Such DM interactions can stabilize the commensurate p -wave magnet, namely the noncollinear zigzag order that has been experimentally observed in $\text{Ni}_2\text{Mo}_3\text{O}_8$ by neutron scattering measurements [74].

While we have focused on the strong-coupling limit in this work, an important open question is whether the p -wave magnet also emerges in the weak-coupling regime. In addition, now that effective spin models realizing the p -wave magnet have been established, a natural next step is to investigate its magnon excitation spectrum and associated dynamical properties. Another promising direction is to examine whether lattice distortions can generate finite DM interactions in Kitaev candidate materials by lifting local inversion symmetry on the relevant bonds. This could provide a route to the additional anisotropic exchanges needed to stabilize commensurate p -wave magnetism. A representative example is the Kitaev material $\beta\text{-Li}_2\text{IrO}_3$, where the presence of weak DM interactions was predicted [75].

Acknowledgments.— We thank Matthew Bunney and Themba Hodge for insightful discussions related to this work. G.B.S. thanks Johannes Knolle, Moon Jip Park, and SungBin Lee for hosting during the initial stage of this work. This work was supported by the Australian Research Council (ARC) through Grants No. DP200101118 and DP240100168. This research was undertaken using resources from the National Computational Infrastructure (NCI Australia), an NCRIS en-

abled capability supported by the Australian Government. Tensor network calculations were performed using the TeNPy Library [76, 77].

* gibaik.sim@unimelb.edu.au

† stephan.rachel@unimelb.edu.au

- [1] T. Moriya, *Spin Fluctuations in Itinerant Electron Magnetism*, edited by P. Fulde, M. Cardona, and H.-J. Queisser, Springer Series in Solid-State Sciences, Vol. 56 (Springer, Berlin, Heidelberg, 1985).
- [2] I. Žutić, J. Fabian, and S. Das Sarma, *Spintronics: Fundamentals and applications*, *Rev. Mod. Phys.* **76**, 323 (2004).
- [3] S. Hayami, M. Yatsushiro, Y. Yanagi, and H. Kusunose, Classification of atomic-scale multipoles under crystallographic point groups and application to linear response tensors, *Phys. Rev. B* **98**, 165110 (2018).
- [4] T. Jungwirth, R. M. Fernandes, E. Fradkin, A. H. MacDonald, J. Sinova, and L. Šmejkal, *Altermagnetism: An unconventional spin-ordered phase of matter*, *Newton* **1**, 100162 (2025).
- [5] M. I. Katsnelson, V. Yu. Irkhin, L. Chioncel, A. I. Lichtenstein, and R. A. De Groot, *Half-metallic ferromagnets: From band structure to many-body effects*, *Rev. Mod. Phys.* **80**, 315 (2008).
- [6] K.-H. Ahn, A. Hariki, K.-W. Lee, and J. Kuneš, Antiferromagnetism in RuO_2 as a d -wave pomeranchuk instability, *Phys. Rev. B* **99**, 184432 (2019).
- [7] S. Hayami, Y. Yanagi, and H. Kusunose, Bottom-up design of spin-split and reshaped electronic band structures in antiferromagnets without spin-orbit coupling: Procedure on the basis of augmented multipoles, *Phys. Rev. B* **102**, 144441 (2020).
- [8] L.-D. Yuan, Z. Wang, J.-W. Luo, E. I. Rashba, and A. Zunger, Giant momentum-dependent spin splitting in centrosymmetric low- Z antiferromagnets, *Phys. Rev. B* **102**, 014422 (2020).
- [9] L. Šmejkal, J. Sinova, and T. Jungwirth, Beyond Conventional Ferromagnetism and Antiferromagnetism: A Phase with Nonrelativistic Spin and Crystal Rotation Symmetry, *Phys. Rev. X* **12**, 031042 (2022).
- [10] L. Šmejkal, J. Sinova, and T. Jungwirth, Emerging Research Landscape of Altermagnetism, *Phys. Rev. X* **12**, 040501 (2022).
- [11] V. Leeb, A. Mook, L. Šmejkal, and J. Knolle, Spontaneous Formation of Altermagnetism from Orbital Ordering, *Phys. Rev. Lett.* **132**, 236701 (2024).
- [12] Y. Li, V. Leeb, K. Wohlfeld, R. Valentí, and J. Knolle, Exploring d -wave magnetism in cuprates from oxygen moments, *Phys. Rev. B* **112**, 125139 (2025).
- [13] P. A. McClarty and J. G. Rau, Landau Theory of Altermagnetism, *Phys. Rev. Lett.* **132**, 176702 (2024).
- [14] L. Šmejkal, A. H. MacDonald, J. Sinova, S. Nakatsuji, and T. Jungwirth, Anomalous Hall antiferromagnets, *Nat Rev Mater* **7**, 482 (2022).
- [15] C. Song, H. Bai, Z. Zhou, L. Han, H. Reichlova, J. H. Dil, J. Liu, X. Chen, and F. Pan, Altermagnets as a new class of functional materials, *Nat Rev Mater* **10**, 473 (2025).
- [16] L. Bai, W. Feng, S. Liu, L. Šmejkal, Y. Mokrousov, and Y. Yao, *Altermagnetism: Exploring New Frontiers in*

- Magnetism and Spintronics, *Advanced Functional Materials* **34**, 2409327 (2024).
- [17] Z. Liu, H. Hu, and X.-J. Liu, *Altermagnetism and Superconductivity: A Short Historical Review*, arXiv:2510.09170 (2025).
- [18] J. E. Hirsch, Spin-split states in metals, *Phys. Rev. B* **41**, 6820 (1990).
- [19] C. Wu and S.-C. Zhang, Dynamic Generation of Spin-Orbit Coupling, *Phys. Rev. Lett.* **93**, 036403 (2004).
- [20] C. M. Varma and L. Zhu, Helicity order: Hidden order parameter in URu₂Si₂, *Phys. Rev. Lett.* **96**, 036405 (2006).
- [21] C. Wu, K. Sun, E. Fradkin, and S.-C. Zhang, Fermi liquid instabilities in the spin channel, *Phys. Rev. B* **75**, 115103 (2007).
- [22] E. I. Kiselev, M. S. Scheurer, P. Wölfle, and J. Schmalian, Limits on dynamically generated spin-orbit coupling: Absence of $l = 1$ pomeranchuk instabilities in metals, *Phys. Rev. B* **95**, 125122 (2017).
- [23] Y.-M. Wu, A. Klein, and A. V. Chubukov, Conditions for $l = 1$ Pomeranchuk instability in a Fermi liquid, *Phys. Rev. B* **97**, 165101 (2018).
- [24] A. B. Hellenes, T. Jungwirth, R. Jaeschke-Ubiergo, A. Chakraborty, J. Sinova, and L. Šmejkal, P-wave magnets, arXiv:2309.01607 (2024).
- [25] A. Chakraborty, A. Birk Hellenes, R. Jaeschke-Ubiergo, T. Jungwirth, L. Šmejkal, and J. Sinova, Highly efficient non-relativistic Edelstein effect in nodal p-wave magnets, *Nat Commun* **16**, 7270 (2025).
- [26] B. Brekke, P. Sukhachov, H. G. Gill, A. Brataas, and J. Linder, Minimal Models and Transport Properties of Unconventional p -Wave Magnets, *Phys. Rev. Lett.* **133**, 236703 (2024).
- [27] Q. Song, S. Stavrić, P. Barone, A. Droghetti, D. S. Antonenko, J. W. F. Venderbos, C. A. Occhialini, B. Ilyas, E. Ergeçen, N. Gedik, S.-W. Cheong, R. M. Fernandes, S. Picozzi, and R. Comin, Electrical switching of a p-wave magnet, *Nature* **642**, 64 (2025).
- [28] R. Yamada, M. T. Birch, P. R. Baral, S. Okumura, R. Nakano, S. Gao, M. Ezawa, T. Nomoto, J. Masell, Y. Ishihara, K. K. Kolincio, I. Belopolski, H. Sagayama, H. Nakao, K. Ohishi, T. Ohhara, R. Kiyonagi, T. Naka-jima, Y. Tokura, T.-h. Arima, Y. Motome, M. M. Hirschmann, and M. Hirschberger, A metallic p-wave magnet with commensurate spin helix, *Nature* **646**, 837 (2025).
- [29] Y. Yu, M. B. Lyngby, T. Shishidou, M. Roig, A. Kreisel, M. Weinert, B. M. Andersen, and D. F. Agterberg, Odd-Parity Magnetism Driven by Antiferromagnetic Exchange, *Phys. Rev. Lett.* **135**, 046701 (2025).
- [30] X. Chen, J. Ren, Y. Zhu, Y. Yu, A. Zhang, P. Liu, J. Li, Y. Liu, C. Li, and Q. Liu, Enumeration and Representation Theory of Spin Space Groups, *Phys. Rev. X* **14**, 031038 (2024).
- [31] Z. Xiao, J. Zhao, Y. Li, R. Shindou, and Z.-D. Song, Spin Space Groups: Full Classification and Applications, *Phys. Rev. X* **14**, 031037 (2024).
- [32] Y. Jiang, Z. Song, T. Zhu, Z. Fang, H. Weng, Z.-X. Liu, J. Yang, and C. Fang, Enumeration of Spin-Space Groups: Toward a Complete Description of Symmetries of Magnetic Orders, *Phys. Rev. X* **14**, 031039 (2024).
- [33] H. Schiff, A. Corticelli, A. Guerreiro, J. Romhányi, and P. A. McClarty, The crystallographic spin point groups and their representations, *SciPost Phys.* **18**, 109 (2025).
- [34] S. Wu, W. A. Phelan, L. Liu, J. R. Morey, J. A. Tutma-her, J. C. Neuefeind, A. Huq, M. B. Stone, M. Feyngenson, D. W. Tam, B. A. Frandsen, B. Trump, C. Wan, S. R. Dunsiger, T. M. McQueen, Y. J. Uemura, and C. L. Bro-holm, Incommensurate Magnetism Near Quantum Criti-cality in CeNiAsO, *Phys. Rev. Lett.* **122**, 197203 (2019).
- [35] F. Lu, X. He, K. Cheng, Z. Wang, J. Zhang, and Y. Luo, ⁷⁵As NMR study of the antiferromagnetic kondo lattice compound ceniaso, *Phys. Rev. B* **107**, 045104 (2023).
- [36] T. Shishidou, D. F. Agterberg, and M. Weinert, Mag-netic fluctuations in single-layer FeSe, *Commun Phys* **1**, 8 (2018).
- [37] R. Stadel, D. D. Khalyavin, P. Manuel, K. Yokoyama, S. Lapidus, M. H. Christensen, R. M. Fernandes, D. Phe-lan, D. Y. Chung, R. Osborn, S. Rosenkranz, and O. Chmaissem, Multiple magnetic orders in lafeas_{1-x}pxo uncover universality of iron-pnictide superconductors, *Commun Phys* **5**, 146 (2022).
- [38] R. Dsouza, A. Kreisel, B. M. Andersen, D. F. Agterberg, and M. H. Christensen, Odd-Parity Magnetism in Fe-Based Superconductors, arXiv:2508.21673 (2025).
- [39] T. Zhu, D. Zhou, H. Wang, and J. Ruan, Floquet odd-parity collinear magnets, arXiv:2508.02542 (2025).
- [40] S. Huang, Z. Qin, F. Zhan, D.-H. Xu, D.-S. Ma, and R. Wang, Light-induced Odd-parity Magnetism in Con-ventional Collinear Antiferromagnets, arXiv:2507.20705 (2025).
- [41] B. Li, D.-F. Shao, and A. A. Kovalev, Floquet Spin Splitting and Spin Generation in Antiferromagnets, arXiv:2507.22884 (2025).
- [42] C. Lee and P. M. R. Brydon, Inversion-Asymmetric Itiner-ant Antiferromagnets by the Space Group Symmetry, *Phys. Rev. Lett.* **135**, 116701 (2025).
- [43] V. Leeb and J. Knolle, Collinear p -wave magnetism and hidden orbital ferrimagnetism, arXiv preprint arXiv:2601.07418 (2026).
- [44] A. H. MacDonald, S. M. Girvin, and D. Yoshioka, T U expansion for the Hubbard model, *Phys. Rev. B* **37**, 9753 (1988).
- [45] L. Shekhtman, O. Entin-Wohlman, and A. Aharony, Moriya's anisotropic superexchange interaction, frustra-tion, and Dzyaloshinsky's weak ferromagnetism, *Phys. Rev. Lett.* **69**, 836 (1992).
- [46] J. Chaloupka, G. Jackeli, and G. Khaliullin, Zigzag mag-netic order in the iridium oxide Na₂IrO₃, *Phys. Rev. Lett.* **110**, 097204 (2013).
- [47] J. G. Rau, E. K.-H. Lee, and H.-Y. Kee, Generic Spin Model for the Honeycomb Iridates beyond the Kitaev Limit, *Phys. Rev. Lett.* **112**, 077204 (2014).
- [48] I. Rousochatzakis, J. Reuther, R. Thomale, S. Rachel, and N. B. Perkins, Phase diagram and quantum order by disorder in the kitaev $K_1 - K_2$ honeycomb magnet, *Phys. Rev. X* **5**, 041035 (2015).
- [49] J. G. Rau, E. K.-H. Lee, and H.-Y. Kee, Spin-Orbit Physics Giving Rise to Novel Phases in Correlated Sys-tems: Iridates and Related Materials, *Annu. Rev. Con-dens. Matter Phys.* **7**, 195 (2016).
- [50] M. Hermanns, I. Kimchi, and J. Knolle, Physics of the Kitaev Model: Fractionalization, Dynamic Correlations, and Material Connections, *Annu. Rev. Condens. Matter Phys.* **9**, 17 (2018).
- [51] Y. Matsuda, T. Shibauchi, and H.-Y. Kee, Kitaev quan-tum spin liquids, *Rev. Mod. Phys.* **97**, 045003 (2025).
- [52] R. Schaffer, S. Bhattacharjee, and Y. B. Kim, Quantum

- phase transition in Heisenberg-Kitaev model, *Physical Review B—Condensed Matter and Materials Physics* **86**, 224417 (2012).
- [53] L.-M. Duan, E. Demler, and M. D. Lukin, Controlling spin exchange interactions of ultracold atoms in optical lattices, *Physical review letters* **91**, 090402 (2003).
- [54] S. Hassan, S. Goyal, R. Shankar, and D. Sénéchal, Quarter-filled Kitaev-Hubbard model: A quantum Hall state in an optical lattice, *Physical Review B—Condensed Matter and Materials Physics* **88**, 045301 (2013).
- [55] J. Faye, D. Sénéchal, and S. Hassan, Topological phases of the Kitaev-Hubbard model at half filling, *Physical Review B* **89**, 115130 (2014).
- [56] T. Sato and F. F. Assaad, Quantum Monte Carlo simulation of generalized Kitaev models, *Physical Review B* **104**, L081106 (2021).
- [57] S. Rachel, Interacting topological insulators: a review, *Rep. Prog. Phys.* **81**, 116501 (2018).
- [58] J. M. Luttinger and L. Tisza, Theory of Dipole Interaction in Crystals, *Phys. Rev.* **70**, 954 (1946).
- [59] S. R. Sklan and C. L. Henley, Nonplanar ground states of frustrated antiferromagnets on an octahedral lattice, *Phys. Rev. B* **88**, 024407 (2013).
- [60] G. Sim and S. Lee, Discovery of a new type of magnetic order on pyrochlore spinels, *Phys. Rev. B* **98**, 014423 (2018).
- [61] C. L. Henley, Ordering due to disorder in a frustrated vector antiferromagnet, *Phys. Rev. Lett.* **62**, 2056 (1989).
- [62] A. V. Chubukov and Th. Jolicoeur, Order-from-disorder phenomena in Heisenberg antiferromagnets on a triangular lattice, *Phys. Rev. B* **46**, 11137 (1992).
- [63] I. P. McCulloch, Infinite size density matrix renormalization group, revisited, arXiv:0804.2509 (2008).
- [64] U. Schollwöck, The density-matrix renormalization group in the age of matrix product states, *Annals of Physics* **326**, 96 (2011).
- [65] F. Freimuth, S. Blügel, and Y. Mokrousov, Spin-orbit torques in Co/Pt(111) and Mn/W(001) magnetic bilayers from first principles, *Phys. Rev. B* **90**, 174423 (2014).
- [66] H. Li, H. Gao, L. P. Zárbo, K. Výborný, X. Wang, I. Garate, F. Doğan, A. Čejchan, J. Sinova, T. Jungwirth, and A. Manchon, Intraband and interband spin-orbit torques in noncentrosymmetric ferromagnets, *Phys. Rev. B* **91**, 134402 (2015).
- [67] M. Offidani, M. Milletari, R. Raimondi, and A. Ferreira, Optimal Charge-to-Spin Conversion in Graphene on Transition-Metal Dichalcogenides, *Phys. Rev. Lett.* **119**, 196801 (2017).
- [68] A. Manchon, J. Železný, I. M. Miron, T. Jungwirth, J. Sinova, A. Thiaville, K. Garello, and P. Gambardella, Current-induced spin-orbit torques in ferromagnetic and antiferromagnetic systems, *Rev. Mod. Phys.* **91**, 035004 (2019).
- [69] J. Železný, Y. Zhang, C. Felser, and B. Yan, Spin-Polarized Current in Noncollinear Antiferromagnets, *Phys. Rev. Lett.* **119**, 187204 (2017).
- [70] G. Gurung, D.-F. Shao, and E. Y. Tsymbal, Transport spin polarization of noncollinear antiferromagnetic antiperovskites, *Phys. Rev. Materials* **5**, 124411 (2021).
- [71] R. González-Hernández, P. Ritzinger, K. Výborný, J. Železný, and A. Manchon, Non-relativistic torque and Edelstein effect in non-collinear magnets, *Nat Commun* **15**, 7663 (2024).
- [72] J. R. Morey, A. Scheie, J. P. Sheckelton, C. M. Brown, and T. M. McQueen, $\text{Ni}_2\text{Mo}_3\text{O}_8$: Complex antiferromagnetic order on a honeycomb lattice, *Phys. Rev. Materials* **3**, 014410 (2019).
- [73] P. Yadav, S. Lee, G. L. Pascut, J. Kim, M. J. Gutmann, X. Xu, B. Gao, S.-W. Cheong, V. Kiryukhin, and S. Choi, Noncollinear magnetic order, in-plane anisotropy, and magnetoelectric coupling in the pyroelectric honeycomb antiferromagnet $\text{Ni}_2\text{Mo}_3\text{O}_8$, *Phys. Rev. Res.* **5**, 033099 (2023).
- [74] B. Gao, T. Chen, X.-C. Wu, M. Flynn, C. Duan, L. Chen, C.-L. Huang, J. Liebman, S. Li, F. Ye, M. B. Stone, A. Podlesnyak, D. L. Abernathy, D. T. Adroja, M. Duc Le, Q. Huang, A. H. Nevidomskyy, E. Morosan, L. Balents, and P. Dai, Diffusive excitonic bands from frustrated triangular sublattice in a singlet-ground-state system, *Nat Commun* **14**, 2051 (2023).
- [75] R. Yadav, S. Rachel, L. Hozoi, J. van den Brink, and G. Jackeli, Strain-and pressure-tuned magnetic interactions in honeycomb Kitaev materials, *Physical Review B* **98**, 121107 (2018).
- [76] J. Hauschild and F. Pollmann, Efficient numerical simulations with Tensor Networks: Tensor Network Python (TeNPy), *SciPost Phys. Lect. Notes* , 5 (2018).
- [77] J. Hauschild, J. Unfried, S. Anand, B. Andrews, M. Bintz, U. Borla, S. Divic, M. Drescher, J. Geiger, M. Hefel, K. Hémerly, W. Kadow, J. Kemp, N. Kirchner, V. S. Liu, G. Moller, D. Parker, M. Rader, A. Romen, S. Scalet, L. Schoonderwoerd, M. Schulz, T. Soejima, P. Thoma, Y. Wu, P. Zechmann, L. Zweng, R. Mong, M. Zaletel, and F. Pollmann, Tensor network Python (TeNPy) version 1, *SciPost Phys. Codebases* , 41 (2024).
- [78] X.-J. Luo, J.-X. Hu, and K. T. Law, Spin Symmetry Criteria for Odd-parity Magnets, arXiv:2510.05512 (2025).

END MATTER

Here, we focus on case (ii), specified by the pattern in Eq. (3), which is directly relevant to the honeycomb magnet $\text{Ni}_2\text{Mo}_3\text{O}_8$. In this material, the magnetically active Ni^{2+} ions occupy inequivalent tetrahedral and octahedral oxygen environments, breaking bond-centered inversion symmetry and thereby permitting finite DM interactions [72, 74]. The resulting classical phase diagram of Eq. (4) is shown in Fig. 4(a) (see Sec. III of the Supplemental Material for details). For small angles $0 < \theta < 0.67$, the ground state is an incommensurate spiral. Increasing θ drives a transition into the p -wave magnet, which is stabilized for $0.67 \leq \theta < 1.25$ and is characterized by the ordering wave vector $\mathbf{Q} = \mathbf{M}$, as indicated by the LT spectrum in Fig. 4(b). Within this regime, the p -wave magnet is classically degenerate with noncoplanar states. Upon further increasing θ , the system enters a coplanar 120° state for $1.25 \leq \theta < \pi/2$, with ordering wave vector $\mathbf{Q} = \mathbf{K}$, as shown in Fig. 4(c). This state may be viewed as a coplanar spiral with spins confined to a plane perpendicular to the [001] axis, where spins on the same sublattice are separated by relative angles of $\pm 2\pi/3$, while the relative orientations between dif-

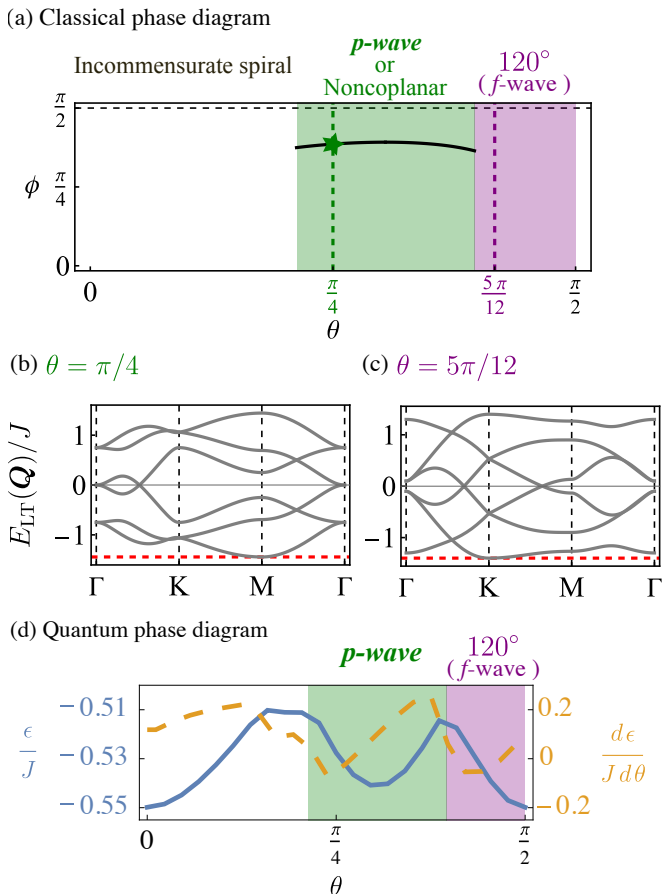


FIG. 4. (a) Classical phase diagram of the model given in Eq. (4) for the $\hat{\mathbf{d}}_i$, specified in Eq. (3). For $0.67 \leq \theta < 1.25$, the model stabilizes the p -wave magnetic state and a competing noncoplanar state, which are energetically degenerate. The canting angle ϕ is defined for the p -wave magnet and quantifies the noncollinearity between the two sublattices. (b,c) Eigenvalue spectra of the LT interaction matrix for $\theta = \pi/4$ and $5\pi/12$. The minimum of the lowest-energy band is located at the M point for the former and at the K point for the latter. (d) Quantum phase diagram of the corresponding spin-1/2 model.

ferent sublattices remain unconstrained. The spin group symmetry of such magnetic order can give rise to an f -wave spin splitting in momentum space [78].

To examine the stability of these states in the quantum limit, we study the spin-1/2 model using iDMRG on an infinite cylinder with $L_x \times L_y \times 2 = 6 \times 3 \times 2$ sites per unit cell (see Sec. IV of the Supplemental Material). This geometry is commensurate with the magnetic unit cells of both the p -wave magnet and the coplanar 120° state, while incommensurate spiral states are suppressed by the finiteness of the unit-cell size. As shown in Fig. 4(d), the ground-state energy per site ϵ develops kinks at $\theta \simeq 0.67$ and 1.25 . Correspondingly, the first derivative $d\epsilon/d\theta$ exhibits two sign changes at these values, signaling first-order phase transitions consistent with the classical phase

diagram. Similar to case (i), quantum fluctuations lift the classical degeneracy and select the p -wave magnet over competing noncoplanar states for $0.67 \leq \theta < 1.25$.

Given that Ni^{2+} ions in $\text{Ni}_2\text{Mo}_3\text{O}_8$ host local spin-1 moments, we further examine a spin-1 extension of Eq. (4) that includes an additional biquadratic exchange term and sublattice-dependent single-ion anisotropy. The latter is motivated by the inequivalent local crystal-field environments of the two Ni sublattices, which allow different anisotropy strengths on sublattices A and B . Our iDMRG results indicate that the single-ion anisotropy primarily induces a sublattice imbalance, thereby rendering the p -wave state ferrimagnetic while preserving the composite symmetry $\mathcal{T}T(\mathbf{t}_1)$ and the spin symmetry $[C_2^\perp || \mathbf{t}_1]$. By contrast, the biquadratic interaction destabilizes the p -wave phase only when it becomes sufficiently large and negative (see Sec. V of the Supplemental Material for details).